Transactions of the Korean Nuclear Society Spring Meeting
Jeju, Korea, May 18-19, 2017

Effect of Chromium Contents on Corrosion Behavior of Ni-Cr-Fe Alloys in PWR Primary Coolant

Hee-Sang Shim, Hyun-Jin Cha, Do Haeng Hur*

Nuclear Materials Safety Research Division, KAERI, 989-111 Daedeok-daero, Yuseong-gu, Daejeon 4057, Korea
**Corresponding author: dhhur@kaeri.re.kr*

1. Introduction

The reduction of occupational radiation exposure is one of the important topics in the water chemistry of nuclear power plants. In a pressurized water reactor (PWR), Co-58 and Co-60 are known as the major sources of the radiation field and produced by a radioactivation of Ni-58 and Co-59, respectively. Ni is released from the surface of various Ni base structural materials such as steam generator tubes and CRDM nozzles because these not only consist of 58-72% nickel but also occupy over 70% of the total surface area exposed to the coolant [1]. Therefore, it is apparent that the mitigation of Ni release from the Ni base alloys should be a crucial strategy for source term reduction in PWRs. Really, since the steam generator tubing material has been replaced from Alloy 600 to Alloy 690, the Co-58 radiation field has been reported to be significantly reduced [2]. This is because the resistance of Ni release is improved in the corrosion environment of PWR primary coolant due to the increase of Cr content.

The diffusion of species into the coolant through the passive layer is depressed due to the increase of the Cr content because increasing Cr content in Ni base alloys enhances the protectiveness of passive film [3-5]. Actually, the passive film, Cr_2O_3, was reported to be stably formed when the Cr content in Ni-Cr-Fe alloys is larger than about 17 wt%, although the critical concentration of Cr for passive film formation depends on many environmental factors such as hydrogen concentration, water chemistry and coolant flow rate. Based on such a background, Alloy 600 (Ni-16Cr-9Fe) and Alloy 690 (Ni-30Cr-9Fe) have been employed as a significant structural material. Thereby, the corrosion characteristics of these materials have been studied in various environmental conditions [6]. However, many works have been focused on stress corrosion cracking researches (SCC) [7,8], and studies on corrosion release in terms of source term reduction have rarely been done.

In this work, the corrosion behaviors of the Ni-Cr-Fe alloys with a different Cr content were investigated in a simulated primary water at 330ºC. The structural properties of these alloys and the properties of corrosion oxide films will be discussed.

2. Experimental

Ni-Cr-Fe alloy materials were melted in a vacuum induction furnace and hot-rolled in a temperature range of 1150~1250ºC. The plates were cold-rolled to a thickness of about 1.5 mm with a total area reduction of about 70%. Cold-worked samples were solution annealed at 1060~1100ºC for 1.5~6 min followed by water quenching to obtain the equivalent grain size and then thermally treated at 715ºC for 10 hr in a vacuum furnace under about 5×10^{-6} torr. The manufacturing condition of the Ni-Cr-Fe alloys with variation of Cr content was summarized in Table 1.

Table 1. Composition, mill annealing temperature and grain size of Ni-Cr-Fe alloys with the variation of Cr content.

Content (wt%)			*Annealing temp. (ºC)*	*Grain size (μm)*
Cr	**Fe**	**Ni**		
16	9	bal.	1060	27.7 ± 2.8
19	9	bal.	1070	28.7 ± 5.0
22	9	bal.	1080	26.7 ± 3.3
25	9	bal.	1090	27.7 ± 3.1
30	9	bal.	1100	28.7 ± 3.2

Corrosion specimens were machined into 15 mm×45 mm×1.5 mm from the each alloy plate and smaller pieces were also cut into 5 mm×5 mm×1.5 mm for a surface oxide analysis. Specimens were finished by grinding with SiC paper of #1200 grit. All specimens were ultrasonically cleaned in acetone, methanol, ethanol, and deionized water in sequence.

The corrosion tests of the Ni-Cr-Fe alloys were conducted using the primary water recirculating system as shown in Fig. 1. 2 ppm Li as lithium hydrate and 1,200 ppm B as boric acid were added into the deionized water to simulate the primary coolant. The dissolved hydrogen and oxygen concentrations were controlled to be 35 $cm^3STP/kg\cdot H_2O$ and lower than 5 ppb, respectively. Corrosion tests were carried out at 330 ºC under 150 bars in the circulating autoclave for 1500 hr.

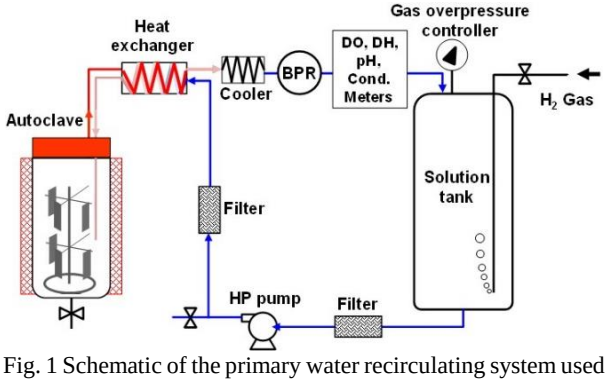

Fig. 1 Schematic of the primary water recirculating system used for the corrosion tests.

Corrosion rate of the Ni-Cr-Fe alloys was evaluated by using gravimetric measurement based on the descale

method. After the corrosion test, the oxidized corrosion specimens were descaled using a two-step alkaline permanganate (AP) and ammonium citrate (AC) process. The first step was a 1% $KMnO_4$ and 5% NaOH solution at 90°C for 30 min, followed by wiping with a cloth. The second step was a 5% ammonium citrate solution at 90 °C for 30 min, followed by wiping with a cloth. After both steps, the weights of the specimens were measured using a 5-place balance with an accuracy of ±0.04 mg. In this way, the two-step descaling process was repeated on each specimen ten times. To correct the base metal losses due to corrosion during the descaling process, the incremental weight losses were reversely linear-extrapolated, according to the ASTM G1-67. Two corrosion specimens (~15 cm^2 per specimen) were used to calculate the corrosion rate of each alloy specimen.

The microstructure of the Ni-Cr-Fe alloys were observed using scanning electron microscopy (SEM). The specimens were etched in a 2% bromine-98% methanol solution to reveal the microstructure. The average grain size was determined through the intercept procedure specified in the ASTM standard [9]. Structural characteristic of Ni-Cr-Fe alloys with a different Cr content was investigated using X-ray diffraction (XRD).

The morphology and chemical composition of the corrosion oxide film formed on the Ni-Cr-Fe alloys with the different Cr content were analyzed using SEM and X-ray photoelectron spectroscopy (XPS). The microstructure and crystallographic property were measured using TEM equipped with EDS and XRD.

3. Results and discussion

The grain size of the Ni-Cr-Fe alloys was equivalently controlled for the increase of Cr content as given in Table 1 and the intergranular carbides (not shown here) were analyzed to be uniformly formed for all alloys. Fig. 2 shows the structural characteristics of the Ni-Cr-Fe alloys obtained using XRD. Two characteristic peaks, (111) and (200), were shifted to a lower 2θ value by increasing of Cr content. The most intense diffraction peak, (111), is gradually varied from 43.84° to 44.12° and second intense peak, (200), is also gradually shifted from 51.04° to 51.31° by the increase of Cr content. This indicates that the lattice is expanded with the addition of Cr content due to the gradual inclusion of the lager "guest" Cr atoms into the lattice of the smaller "host" Ni atoms. In addition, a gradual change in characteristic peaks means that the Cr species are alloyed homogeneously into the Ni-Cr-Fe alloy.

Fig. 3 shows the general corrosion rates of the Ni-Cr-Fe alloys with the variation of Cr content. The corrosion rate of the 16Cr alloy specimen revealed the highest value of 0.96 mg/m^2h, whereas that of the 30Cr alloy specimen showed the lowest value of 0.11 mg/m^2h. Thus, the corrosion rate was lowered by about 88% due to the increase of Cr amount from 16 to 30 wt%. However, no difference was found in the Ni-Cr-Fe alloys with the Cr content more than 22 wt%. This indicates that the Cr content in the Ni-Cr-Fe alloys has the critical value for the resistance of general corrosion in PWR primary coolant. In addition, the release rate from the corroded surface is expected to decrease in proportion to the corrosion rate, referring to theoretical backgrounds and plant data of some literatures [2,10,11].

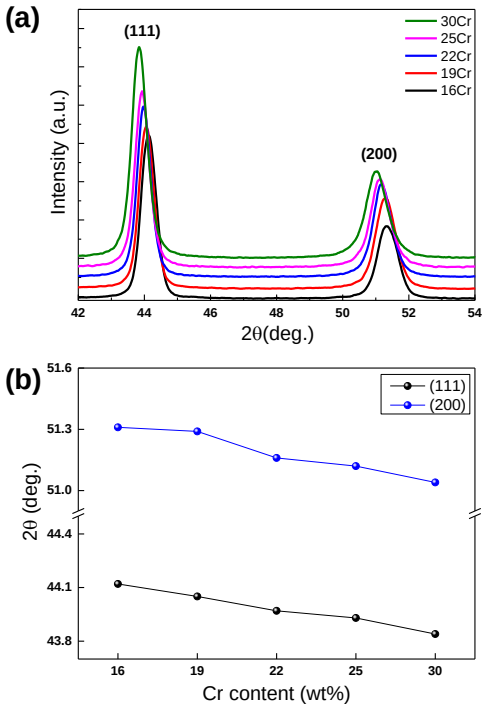

Fig. 2 (a) XRD patterns and (b) the characteristic peak shift of Ni-Cr-Fe alloys with the variation of Cr content.

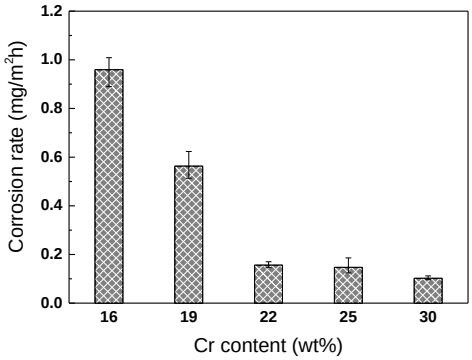

Fig. 3. Corrosion rates of the Ni-Cr-Fe alloys with the variation of Cr content.

Fig. 4 shows the SEM micrographs of the oxidized surface on the Ni-Cr-Fe alloys with a different Cr content. The oxide morphologies formed during the corrosion test of the Ni-Cr-Fe alloys show a clear difference with the increase of the Cr content. The needle-like and strip-like oxides were mainly observed on the 16Cr, 19Cr and 22Cr alloy specimens, whereas the polyhedral particles were dominantly found on the 25Cr and 30Cr alloy specimens, which have relatively high Cr content. In addition, the needle-like and strip-like oxides seem to be grown on the polyhedral particles as shown in Figs. 4(a)~4(c). Particularly, considering that short needle-like oxides were found on the polyhedral oxide layer in the 25Cr

alloy specimen as shown in Fig. 4(d), it is believed that the needle-like and strip-like oxides are started to grow by source supply from the coolant after the polyhedral particles are formed. The density of nanoscaled needle-like and strip-like oxides is gradually decreased by increase of Cr content in alloy. As a result, the thickness of the oxide film decreases, which can have directly contributed to the reduction in the corrosion rate, as the Cr amount in the Ni-Cr-Fe alloys increases.

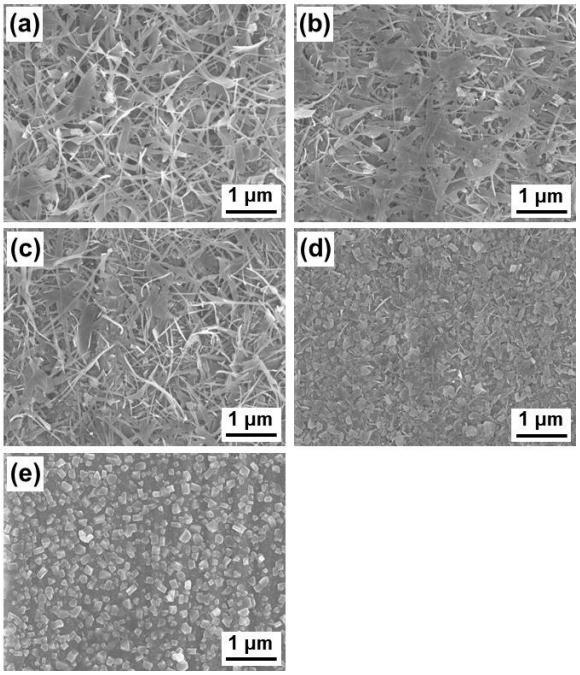

Fig. 4. SEM images of corrosion products formed on Ni-Cr-Fe alloys with the variation of Cr content: (a) 16Cr, (b) 19Cr, (c) 22Cr, (d) 25Cr and (e) 30Cr.

To further analyze the effect of the Cr content on the corrosion oxides of the Ni-Cr-Fe alloys, STEM and EDS area mapping were conducted for the cross-section of the 16Cr and 30Cr corrosion specimens as shown in Fig. 5. The corrosion oxide film of the 16Cr alloy had a triple-layer structure as shown in Fig. 5(a) and 5(b). The chromium oxide (Cr_2O_3) not only was formed as a passive layer between the matrix and outer oxides but also penetrated inside the matrix in some region, splitting a part of the matrix into several pieces. The intermediate layer consists of polyhedral particles of the $(Ni, Cr)_xFe_{3-x}O_4$ spinel phase and the needle-like Ni-rich oxides of $(Fe, Cr)_xNi_{1-x}O$ phase. In addition, only the needle-like oxides were presented in the outmost region. Whereas the corrosion oxide film of the 30Cr alloy had a double-layer structure as shown in Fig. 5(c) and 5(d). The Cr_2O_3 layer was formed with 20~30 nm thickness as an inner oxide and the polyhedral particles of the $(Ni, Cr)_xFe_{3-x}O_4$ spinel phase were formed with a 150~200 nm size on the Cr_2O_3 passive layer. Total thickness of the corrosion oxide layer was about a 600~700 nm for the 16Cr alloy and smaller than 200 nm for the 30Cr alloy. These results indicate that the needle-like oxides of Ni-rich phase are relatively easy to be formed and the protectiveness of the passive film is also poor for the lower Cr alloy. Therefore, the corrosion rate of the 16Cr alloy become much larger than that of the 30Cr alloy.

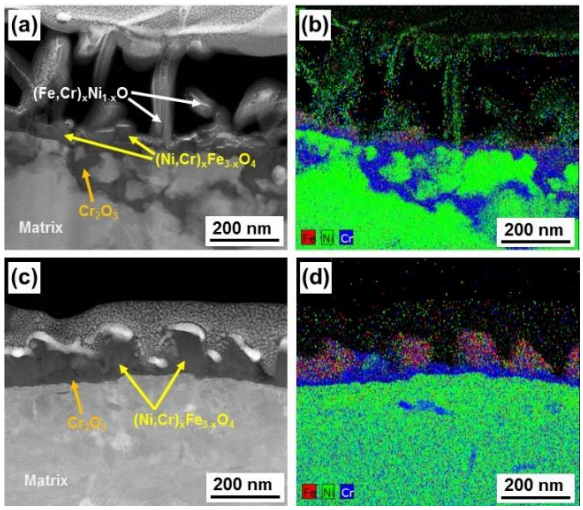

Fig. 5. STEM and EDS area mapping images: (a), (b) the 16Cr alloy and (c), (d) the 30Cr alloy.

4. Conclusions

We investigated the effect of Cr content in the Ni-Cr-Fe alloys on corrosion rate and its oxide formation behavior in PWR primary water. The corrosion rate was reduced by about 88% with the increase of Cr content from 16 wt% to 30 wt%. The Ni-rich needle-like and strip-like oxides were dominantly formed and the protectiveness of the Cr_2O_3 passive film was reduced as the Cr content decreased. In addition, the amount of Cr content in the Ni-Cr-Fe alloys showed a threshold value of more than 22wt% for corrosion rate. Therefore, the use of the Ni-Cr-Fe alloy with a high Cr content is more advantageous in terms of general corrosion and release for source term reduction.

Acknowledgments

This work was supported by the National Research Foundation of Korea (NRF) grant funded by the Korea government (MSIP) (2017M2A8A4015159).

REFERENCES

[1] D. Hussey, Source term Reduction: Impact of Plant Design and Chemistry on PWR Shutdown Releases and Dose Rates, EPRI, Palo Alto, CA, USA, 1013507, 2006.
[2] T. Terachi, T. Kuge, Y. Tsujiie, K. Yamaguchi, T. Nakagawa, M. Murashita, T. Tanabe, S. Tsuji, S. Kawamura, T. Miyawaki, Long-Term Trends in Steam Generator Dose Rates of 11 PWRs, Water Chemistry and Corrosion in Nuclear Power Plants in Asia, Taichung, Taiwan, 2013.
[3] T. Angeliu, G. Was, The effect of chromium, carbon, and yttrium on the oxidation of nickel base alloys in high temperature water, J. Electrochem. Soc. Vol.14, p1877, 1993.
[4] F. Delabrouille, Characterization of cracks of SCC of Ni-base alloys using MET: Effect of chromium content and environment chemistry, INP Toulouse, France, 2004.

[5] J. Panter, Study of stress corrosion cracking of Alloy 690 and Alloy 600 in PWR primary water: Influence of fabrication process of steam generator pipes on the initiation, INP Toulouse, France, 2002.
[6] R. Staehle, Corrosion Basics in Primary and Secondary Systems of LWRs, Advance Test Reactor National Scientific User Facility, User Week, Idaho Falls, ID, 2009.
[7] P. M. Scott, Stress Corrosion Cracking in Pressurized Water Reactors-Interpretation, Modeling, and Remedies, Corrosion, Vol. 56, p.771, 2000.
[8] S. Fyfitch, Corrosion and Stress Corrosion Cracking of Ni-Base Alloys, Comprehensive Nuclear Materials Vol. 5, p.69, 2012.
[9] Standard Test Methods for Determining Average Grain Size, ASTM E112-10, ASTM, 2010.
[10] B. Cheng, Impact of PWR Primary Chemistry on Corrosion Product Deposition on Fuel Cladding Surfaces, EPRI, Palo Alto, CA, USA, TR-108783, 1997.
[11] L. Guinard, O. Kerrec, D. Noel, S. Gardey, F. Coulet, Influence of the initial surface condition on the release of nickel alloys in the primary circuit of PWRs, EDF, France, 97NB00045, 1997.